Journal of the Brazilian Society of Mechanical Sciences and Engineering (2024) 46:452
https://doi.org/10.1007/s40430-024-05027-1

TECHNICAL PAPER

A study on end mill tool geometry parameters for end milling of 316L: finite element analysis and response surface methodology optimization based on resultant cutting force

Semih Yuksel[1,2] · Tolga Berkay Sirin[3] · Mustafa Ay[4] · Mehmet Uçar[5] · Mustafa Kurt[4]

Received: 6 February 2024 / Accepted: 27 May 2024 / Published online: 13 June 2024

Abstract
Advanced tool designs are essential for harnessing the full potential of end milling techniques, which have long served as a cornerstone of the industry. Due to the unique difficulties of designing end milling tools, where many parameters interact in complex ways, it is important to be aware of the limits of relying only on experiments and human judgment to find the best cutting tool geometry. Consequently, advanced data analytics techniques, computational analyses, and optimization strategies play a critical role in this process. Currently, there is a lack of comprehensive studies that thoroughly investigate the impact of end mill geometry on milling 316L stainless steel, considering eight parameters at three different levels and their effects on resultant cutting forces. To address this gap, this research adopts a holistic approach by integrating finite element analysis (FEA), response surface methodology (RSM), and analysis of variance (ANOVA) to develop a predictive model that evaluates the effects of geometric parameters on the resultant cutting forces. The findings indicate that the radial relief angle significantly influences the resultant cutting force, marking it the most critical design parameter. The model effectively predicts cutting forces with a reasonable degree of accuracy, as evidenced by a R^2 value of 83.96% and an adjusted R^2 value of 69.92%. Notably, the resultant cutting force, optimized to 288.73 N, showed a substantial decrease —approximately threefold compared to preliminary experimental results— highlighting the effectiveness of our model and approach.

Keywords End milling · Tool geometry · Tool design · Finite element analysis · Response surface methodology · Analysis of variance

1 Introduction

End milling is a fundamental and crucial material removal process used to manufacture high-quality components with complex free-form surfaces [1]. The mold and die, automotive, aerospace, and medical manufacturing industries extensively use this technique due to its versatility, high productivity, efficiency, ability to process a wide range of materials, and high geometric accuracy and surface quality [2–4]. Effective end milling primarily involves careful consideration of the material, machine tool, process type, process parameters, and tool design [5]. Unlike other processes, the knowledge of which material will be machined is the most critical factor that shapes the milling process, as different materials require specific parameters and conditions for optimal performance [6]. Consequently, specialized end mill tool geometries are preferred for different materials to enhance performance and increase the competitiveness of manufacturing industries [7].

Technical Editor: Lincoln Cardoso Brandao.

✉ Semih Yuksel
semihyuksel@yandex.com

[1] Department of Mechanical Engineering, Institute of Pure and Applied Sciences, Marmara University, 34722 Istanbul, Turkey

[2] Unirobotics Robotik Sistemler A.S, 34775 Istanbul, Turkey

[3] Department of Marine Engineering, Faculty of Maritime, Bandırma Onyedi Eylül University, 10200 Balıkesir, Turkey

[4] Department of Mechanical Engineering, Faculty of Technology, Marmara University, 34722 Istanbul, Turkey

[5] Department of Automotive Engineering, Faculty of Technology, Kocaeli University, 41001 Kocaeli, Turkey

The end mill is one of the most essential, highly accurate, and productive universal cutting tools, developed with various geometric parameters to machine complex-shaped components [8, 9]. The geometry of an end mill has a significant influence on the tool's machining performance characteristics, such as cutting forces, chip formation, and overall machining efficiency [10, 11]. The interaction of the cutting tool with the workpiece and the resultant cutting forces are closely related [12]. Analyzing these forces is crucial for determining power requirements, machining efficiency, tool performance, and preventing chatter vibrations [13]. High cutting forces during an unoptimized machining process can cause tool deflection, wear, high temperatures, residual stresses, and vibrations, which negatively impact the quality of the component [14, 15]. Each cutting edge of the end milling tool experiences these forces, with the resultant milling force being the vector sum of the three orthogonal components exposed to each cutting edge: the main cutting force F_c, the back force F_p, and the axial force F_a [16]. Understanding the significance of the total resultant force is crucial, as it directly correlates with tool wear, deflection, and overall machining quality.

Cutting forces are critical in determining and evaluating the specific geometries and designs of different end milling tools [15]. Therefore, modifying tool geometry is an effective method for optimizing these forces [11, 13]. The literature reveals a notable gap in studies investigating the effects of end mill tool geometry on cutting forces. The competitive nature of the global cutting tool manufacturing industry often keeps such knowledge secret and limits technological development. Thus, exploring the existing literature and conducting comprehensive studies to address this gap are valuable. Joshi et al. [17], investigated the effect of end mill geometry on milling force and surface integrity. According to their study, it is possible to manipulate and reduce cutting forces by optimizing tool geometry parameters such as the number of flutes, helix angle, and tool diameter. The study also concluded that surface integrity had improved. Ren et al. [18] explored the multi-objective optimization of cutter geometric parameters during the end milling of Ti–5Al–5Mo–5V–1Cr–1Fe titanium alloy, utilizing the Taguchi method integrated with gray relational analysis. Sethupathy and Shanmugasundaram [19] used response surface methodology, experimental design, and analysis of variance to predict cutting forces based on geometric and machining parameters. Ma et al. [20] analyzed tool wear and cutting forces in high-speed milling of Inconel 718 curved surfaces, finding that variations in cutting force followed the same trends as tool wear, and that the cutting tool geometric parameters significantly affected tool wear and life. Subramanian et al. [21] applied response surface methodology to optimize geometric and machining parameters in order to predict vibration amplitude. Aslantas and Alatrushi [22] examined the impact of tool geometry on cutting forces, surface roughness, and burr formation in the micromilling process. Tang et al. [23] conducted a comprehensive investigation of milling parameters and milling tool parameters through orthogonal experimental design and subsequent finite element analysis. Ji et al. [24] proposed a new model for predicting cutting temperature in Al7050 milling that considers both tool geometry and milling parameters, discovering a polynomial relationship between tool geometric parameters and cutting temperature. In addition, Ahmed et al. [25], Zhang et al. [26], Wang et al. [27], Doluk et al. [28], Narooei et al. [29], Izamshah et al. [30], Monka et al. [31], Zhang et al. [32], and Kusyi et al. [33] also conducted studies on the geometric parameters of end milling tools.

Designing end mills is a complex task, especially when tailored for specific applications [34]. It is challenging to optimize parameters and select the best alternative tools based solely on experimental test plans and human decision-making. Designing a customized cutting tool involves balancing time constraints, applicability, capacity, financial implications, and environmental sustainability. Inadequate cutter selection can lead to unfeasible and inconsistent process plans [8]. Therefore, a comprehensive strategy to predict and optimize the most suitable end mill geometry parameters for the designed process plan is indispensable.

The literature includes research on optimizing end milling cutting parameters (such as cutting speed, feed rate, and depth of cut) for a variety of materials, including 316L stainless steel. These studies typically employ an array of mathematical, experimental, AI-based, and hybrid modeling techniques, including finite element analysis, the Taguchi method, response surface methodology, gray relational analysis, analysis of variance, artificial neural networks, and genetic algorithms [35]. However, most of the existing studies are limited and superficial, often focusing solely on a restricted number of cutter geometry parameters in addition to cutting parameters. Yet, it is evident that a comprehensive model cannot be achieved without considering all geometric parameters. Additionally, it remains unclear how tool geometric parameters affect the total cutting force. However, there is no research available that comprehensively optimizes the geometric parameters of any end milling tool for machining 316L. Further research on cutting tools with different geometric parameters is urgently needed to improve the efficiency of machining 316L. Moreover, there are very few models that consider the effect of the geometric structure of the end milling tool on the cutting force resulting from milling, and few scientists have conducted research on the relationship between the geometric structure of the end milling tool and the cutting force resulting from milling. Therefore, the novelty of this work lies in its holistic approach to optimizing eight end mill tool geometry parameters based on total cutting force, utilizing a simulation model, for

machining 316L stainless steel, a material that poses significant machining challenges. It uniquely integrates finite element analysis (FEA), response surface methodology (RSM), and analysis of variance (ANOVA) to develop a predictive model by evaluating the effects of geometric parameters on the resultant cutting forces. The research has been done to explore the impact of tool geometric parameters on milling force. A novel milling force model was developed using finite element simulation, incorporating a mathematical model, tool geometric parameters, and milling parameters. This approach not only increases tool design precision, but also significantly reduces the experimental burden typically required in tool optimization processes. Advances in this overdue research will make a significant contribution to the field of machining, especially in high-risk industries where 316L stainless steel is common.

2 Materials and methods

The stainless steel AISI (American Iron and Steel Institute) 316L material was chosen for the research due to its significant importance across various sectors such as energy, biomedical, maritime, aeronautical, and automotive, attributed to its superior properties [36]. Notably, these properties include exceptional corrosion resistance, antibacterial qualities, superior mechanical strength, biocompatibility, cost-effectiveness, and wide availability [37–41]. Grade 316L is prone to work hardening and has low thermal conductivity [39, 42]. Additionally, under high cutting speeds and thermal loads, chips tend to adhere strongly to the tool insert, making 316L a difficult-to-machine material [39, 43]. This necessitates strategies to minimize work hardening, properly distribute heat, and ensure optimal efficiency and tool longevity during the milling process [43]. One basic approach is to immediately replace worn and no longer sharp cutting tools, whereas a more effective strategy involves using specially designed and optimized cutting tool geometries [43]. Test samples were precisely manufactured with dimensions of 140 (L) x 150 (W) x 150 (H) mm. Table 1 presents a comprehensive chemical composition analysis of AISI 316L, while Table 2 details the mechanical properties.

All experiments and measurements in this study were meticulously conducted using advanced equipment and software resources at the facilities of Karcan Cutting Tools Industry and Trade Inc. The machining experimental tests were executed with precision on a Mikron VCP800 3-axis CNC (Computer Numerical Control) milling machine. The assessment of cutting forces, torsion moments, and bending moments along three axes was recorded using the remote data acquisition sensor, Spike Mobile 1.2. The imperative need for data accuracy and reliability underpinned this selection, further reinforcing the robustness of the research findings. Figure 1 presents the workpiece material and the Spike Mobile 1.2 sensor.

Table 2 Mechanical properties of AISI 316L [45]

Tensile strength (MPa)	Yield strength (MPa)	Vickers hardness (HV)	Elastic modulus (GPa)	Elongation (% in 50 mm)	Density (g/cm^3)
650	280	190	211	45	7.90

2.1 Preliminary experimental tests

Preliminary experimental tests play an integral role in the calibration and validation of parameters used in finite element analysis. These tests are not only essential but also indispensable for accurately defining the parameters, consequently enhancing accuracy, consistency, and predictability. This approach helps establish a closer correspondence between experimental and analytical outcomes. Two sample end mill tools (named Tool 1 and Tool 2), suitable for use in preliminary experimental tests, were selected from the comprehensive inventory used by our collaborative partner in processing 316L material. The tools are made from cemented carbide rods of grade CTS20D (WC/Co) by Ceratizit Company, which correspond to ISO grade K20-K40, and are coated with AlCrXN-based (Oerlikon Balzers Alnova) material. Subsequently, the results of the preliminary experimental tests with these two sample cutting tools were compared with finite element analysis findings to check for accuracy and convergence. The tests were carried out in five repeats with a maximum error range of $\pm 5\%$, and the arithmetic average of the values was calculated. Figure 2 includes technical schematics that elucidate the design and geometry of the employed cutting tools for visual reference. Table 3 comprehensively documents the end mill tool parameter values.

Preliminary experimental tests were conducted under dry cutting conditions using the down-milling technique, strictly adhering to the guidelines specified in the test standards. A

Table 1 Chemical composition analysis results of AISI 316L (wt% weight percentage, Bal.-balance.) [44]

Element	Cr	Ni	Mo	C	Mn	P	S	Si	N	Fe
(wt%)	18.0	14.0	2.85	0.03	2.0	0.025	0.03	0.75	0.1	Bal

Fig. 1 Workpiece material (**a**) and Spike mobile 1.2 (**b**)

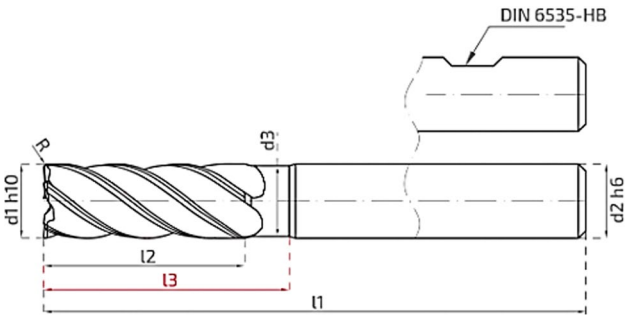

Fig. 2 Design and geometry of the sample end mill tools

12 mm diameter cutting tool was used for a total cutting length of 150 mm. The down-milling process is illustrated in Fig. 3.

Preliminary experimental tests were conducted using the provided sample cutting tools, following the cutting parameters outlined in Table 4. The acquired data underwent comparative analysis. This examination revealed a strong alignment between the cutting forces obtained in the tests and those predicted by finite element analysis. Both tests and finite element analysis, carried out with the parameters in the table, achieved convergence with an acceptable percentage of error, as shown in Eq. (1). Therefore, these parameters were considered appropriate and were subsequently used in the finite element analysis. Consequently, the decision was made to continue with Tool 1, which produced lower cutting forces despite a higher error rate.

$$\text{Percentage error} = \left| \frac{F_{\text{experiment}} - F_{\text{FEA}}}{F_{\text{experiment}}} \right| \times 100 \tag{1}$$

2.2 Response surface methodology model and analysis of variance

George E. P. Box and K. B. Wilson proposed Response Surface Methodology (RSM) in 1951, employing mathematical and statistical techniques to analyze problems with an empirical model [46–48]. RSM aims to establish a relationship between a target response and the varying levels of a defined set of input variables or factors, with the ultimate goal of optimizing this response [49, 50]. The integration of response surface methods with parameter design has become a robust optimization tool across various engineering applications [51, 52]. The most commonly used response models are linear and quadratic, typically expressed as follows [53]:

The first-order (linear) model,

$$y = \beta_0 + \beta_1 X_1 + \beta_2 X_2 + \cdots + \beta_K X_K + \varepsilon \tag{2}$$

where K represents the number of variables and ε denotes the error term.

The second-order (quadratic) model,

$$y = \beta_0 + \sum_{i=1}^{K} \beta_i X_i + \sum_{i=1}^{K} \beta_{ii} X_i^2 + \sum \sum_{i<j} \beta_{ij} X_i X_j + \varepsilon \tag{3}$$

The error (or residual) is the difference between the observed response values and the predicted values obtained from the linear regression model. Mathematically, the error for each data point i is calculated as:

$$e_i = y_i - \hat{y}_i \tag{4}$$

Sum of Squared Errors (SSE): This is the sum of the squared errors:

Table 3 Variable values of the sample end mill tools

Variables	Tool 1	Tool 2
Tool diameter	12 mm	12 mm
flute	5	6
Core diameter	7.5 mm	6.3–7.65 mm (tapered)
Radial rake angle	4°–6°	6°–8°
Helix angle	42°	38°
Radial relief angle	7°–9°	10°–12°
Axial relief angle	7°–9°	10°–12°
Edge radius	1.0 mm	0.5 mm
Flute radius	1.6–1.7 mm	1.9–2.0 mm
Width of land	1.2–1.3 mm	1.8–1.9 mm

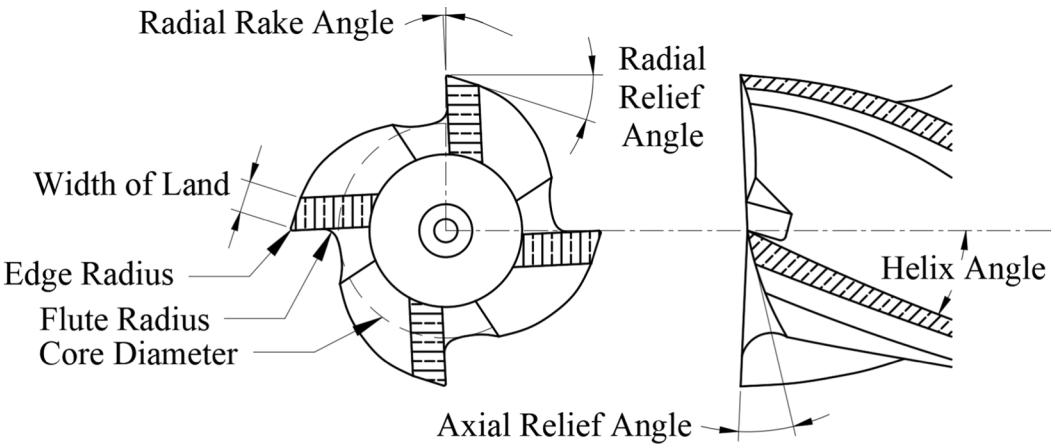

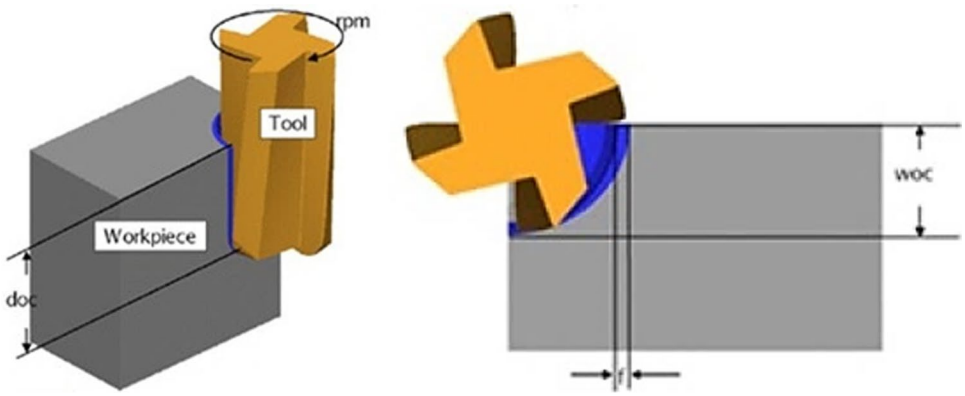

Fig. 3 Schematic of down-milling process (DOC: depth of cut, WOC: width of cut)

Table 4 Comparison of preliminary experimental tests and finite element analysis

Tools	Cutting speed, V_c, (m/min)	Feed per tooth, f_z, (mm/tooth)	Axial depth of cut, a_p, (mm)	Radial depth of cut, a_e, (mm)	Cutting force of exp., N	Cutting force of FEA, N	Error,%
Tool 1	70	0.08	20	1.2	973.7917	750.062	22.97511
Tool 2					1119.329	1029.5	8.02526

$$\mathrm{SSE} = \sum_{i=1}^{n} \left(y_i - \hat{y}_i\right)^2 \tag{5}$$

Mean Squared Error (MSE): The average of the SSE, divided by the number of observations:

$$\mathrm{MSE} = \frac{1}{n} \sum_{i=1}^{n} \left(y_i - \hat{y}_i\right)^2 \tag{6}$$

Root Mean Squared Error (RMSE): The square root of the MSE, which gives an error metric in the same units as the dependent variable:

$$\mathrm{RMSE} = \sqrt{\frac{1}{n} \sum_{i=1}^{n} \left(y_i - \hat{y}_i\right)^2} \tag{7}$$

where ε denotes the observed error in response y, the expected response is represented as $y - \varepsilon$, the b's are the regression coefficients to be estimated, e_i is the error for the ith observation, y_i is the observed response value for the ith observation, and $\hat{y}_i$ is the predicted response value for the ith observation obtained from the linear regression model.

It is crucial to test the statistical significance of calculated coefficients or model equations using Analysis of Variance (ANOVA), which verifies the model's adequacy concerning the experiment's responses [54]. The F-value and P-value in ANOVA are vital for interpreting results and drawing conclusions from statistical analysis. A high F-value indicates significant differences among group means, while the P-value, associated with the F-test, signifies the probability of obtaining observed results, or more extreme, under the null hypothesis that no real differences exist among group means [55–58]. A low P-value (typically less than 0.05) suggests that the observed differences are statistically significant, leading researchers to reject the null hypothesis if the P-value is below the chosen significance level, often set at 0.05 [59–61]. In this study, ANOVA was used to identify significant end mill tool design parameters and their interactions affecting the resultant cutting force, with a significance level of $\alpha = 0.05$ or a confidence interval of 95%. Parameters and interactions with a P-value less than 0.05 are considered significant [62].

Acquiring optimal values for end mill tool geometry parameters, which significantly influence the resultant cutting force, is exceptionally challenging without mathematical and statistical techniques. Milling a specific material with a tool characterized by generic geometry, material, and coating, along with unspecified parameters and types of milling operations, would require an impractical number of tests, potentially reaching millions for each material. Hence, the application of the finite element analysis, the response surface method, and the analysis of variance is crucial to optimizing end mill tool geometry parameter values with the fewest experiments possible.

The complexity of this research required a total of 6561 (3^8) experiments involving 8 end mill tool geometry variables, each categorized into three distinct levels (L1—low, L2—mid, and L3—high). The use of a 3-level (− 1, 0, and 1 correspond to L1, L2, and L3 respectively) and 8-factor central composite design minimizes the required number of tests. Specifically, employing a fractional reduction for cube points in the test plan reduced

Table 5 Factors and factor levels used in the analysis

Factors	L1	L2	L3
Core diameter	6.75	6.975	7.2
Radial rake angle	5	7	9
Helix angle	34	36	38
Radial relief angle	9	11	13
Axial relief angle	7	9	11
Edge radius	0.5	0.7	0.9
Flute radius	1.85	1.95	2.05
Width of land	1.65	1.75	1.85

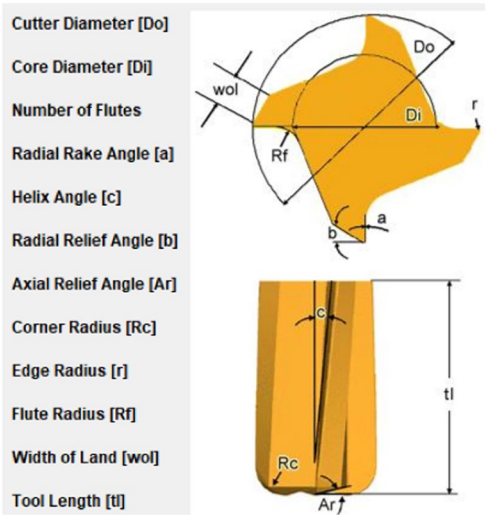

the number of test configurations to 158 (97 when excluding redundant repetitions). This reduction was achieved from an initial pool of 6561 possibilities considered in a complete fractional test plan. Table 5 displays the 8 factors associated with the end mill cutting tool, along with their respective three levels, and Table 6 illustrates the central composite design matrix used in this study.

Our study was underpinned by the computational capabilities of multiple systems, enabling seamless execution of complex experimental designs while ensuring realistic validations and convergences. The experimental data was processed through Matlab R2023a software, yielding the total resultant cutting forces. These 97 distinct experiments were expanded to a full factorial configuration within the experimental design to assess the total resultant cutting forces. This approach allowed us to adopt a predictive methodology, creating predictions for the full complement of the 6561 experiments initially required. These parameters were selected through a collaborative process with our industry partner, emphasizing their suitability for manufacturability. Furthermore, the values were derived from an exhaustive averaging of critical production tolerances. Response surface methodology and analysis of variance were conducted using Minitab 21.4 software, and results were rigorously interpreted through the extensive capabilities of Matlab R2023a.

2.3 The custom finite element analysis (FEM) modeling

Finite element analysis was conducted using Advantage v7.1 software, where the variable values of the end mill cutting tool and the workpiece were defined. In finite element analysis, the reference point is the initiation of mean cutting forces after a single revolution of the cutting tool, considering relevant feed rate, revolution, and cutting speed parameters. The initial temperature for the analysis was set at 20 °C.

Meshing definitions for the tool are set at 10, 0.5, and 0.35 for maximum element size, minimum element size, and mesh grading, respectively. Similarly, meshing definitions for the workpiece are set at 45, 0.4, and 0.35 for maximum element size, minimum element size, and mesh grading, respectively. Additionally, the minimum element edge length for the workpiece is set at 0.012 mm. The dimensions of the workpiece are determined to be 6 mm (width) × 8 mm (height) × 10 mm (length). Adaptive meshing tools have been employed to minimize distortion in the mesh.

Boundary conditions were established, and the dimensional properties of the simulated tool were defined based on the tool used in the experimental work. The end mill tool is considered rigid and was meshed, comprising 14,780 elements. The workpiece, modeled with 615,890 elements, was also meshed. To ensure the accuracy and reliability of simulation results, the mesh of the structure has been refined until the results become independent of the mesh size. Initially,

Table 6 RSM central composite design (CCD) matrix

Run	Blk	Coded variables								Code
		A	B	C	D	E	F	G	H	
1	1	1	−1	−1	−1	1	1	−1	1	$A_3B_1C_1D_1E_3F_3G_1H_3$
2	1	1	−1	1	1	−1	−1	−1	1	$A_3B_1C_3D_3E_1F_1G_1H_3$
3	1	1	−1	−1	−1	1	1	1	−1	·
4	1	−1	1	−1	−1	−1	−1	1	−1	·
5	1	−1	−1	1	−1	−1	1	−1	−1	·
6	1	−1	−1	−1	1	−1	1	−1	−1	·
7	1	1	−1	−1	−1	−1	−1	−1	1	·
8	1	0	0	0	0	0	0	0	0	·
9	1	1	−1	−1	−1	−1	−1	1	−1	·
10	1	−1	1	1	1	1	1	1	−1	·
.										.
.										.
.										.
.										.
.										.
156	5	0	0	0	0	0	0	0	0	·
157	5	0	0	0	0	0	0	0	0	·
158	5	0	0	0	0	0	0	1	0	·
159	5	0	0	0	−1	0	0	0	0	·
160	5	0	0	0	0	0	0	0	1	$A_2B_2C_2D_2E_2F_2G_2H_3$

Table 7 Features, boundary conditions and meshing for tool and workpiece in Advantage

V	Workpiece	Tool
Young's modulus, (GPa)	200	650
Poisson's ratio,(*y*)	0.3	0.2
Constant friction, (m)	0.5	0.5

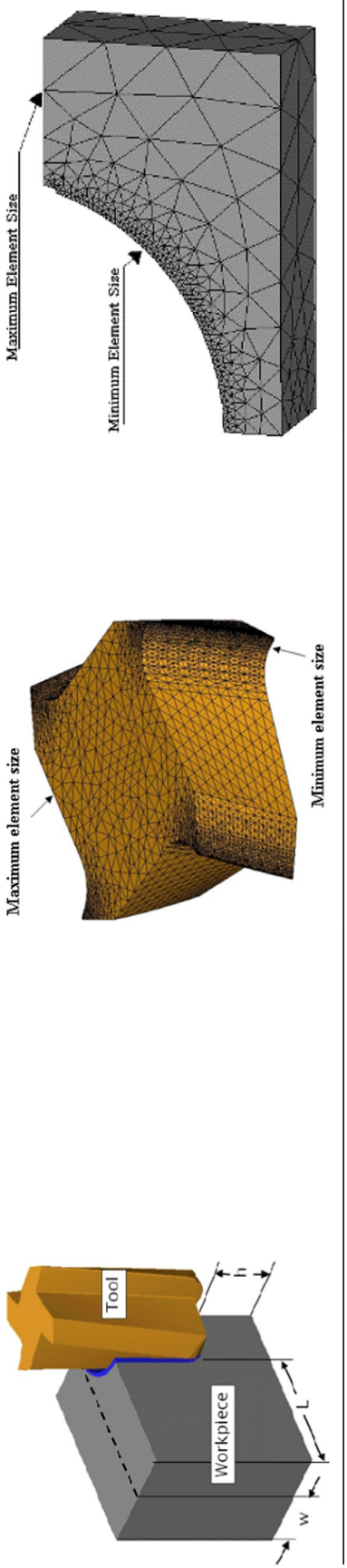

the simulation was conducted with a coarse mesh to gain a basic understanding of the model's behavior under specified conditions. The mesh was systematically refined by reducing the element size, which increased the total number of elements. This refinement was typically focused on areas where high variations in the results were observed. After refining the mesh, the analysis was performed again. The results from the refined mesh were compared with those from the coarser mesh. As a result of convergence, the regions cut by the refined mesh were more precisely delineated, whereas the effects in regions meshed coarsely were less significant. Therefore, adaptive mesh refinement was applied to the workpiece. Once convergence was achieved, it was confirmed that the mesh was fine enough to capture the critical phenomena in the analysis, ensuring that the results were not influenced by the size or distribution of the mesh. The final mesh was then used in all subsequent analyses, as further refinement would only increase computational time without affecting the outcomes. The properties specified in Table 7 were used for both the workpiece and cutting tool in the simulation.

3 Results and analysis

The effects of cutting tool parameters on the selected response variable were evaluated for AISI 316L material using the experiments outlined previously. The results were processed in Minitab software for further analysis. A quadratic model was developed to describe the relationship between the resultant cutting force and cutting tool variables. Analysis of variance (ANOVA) was employed to assess the adequacy of this model. The results for the AISI 316L material are presented accordingly.

The adequacy of the models and the significance of individual model coefficients were examined through the analysis of variance and the *F*-ratio test. Table 8 displays the ANOVA table for the proposed model, corresponding to the resultant cutting force presented in Eq. 3. A *P*-value below 0.05 indicates that the model is statistically significant at the 95% confidence level. Furthermore, the calculated *F*-ratio, which exceeds the standard *F*-ratio value of 1.472, indicates that the model adequately depicts the relationship between the resultant cutting force response and the end mill design parameters at a 95% confidence level.

It's clear from the ANOVA table for individual model coefficients that some effects, like the radial relief angle and radial rake angle, are important at the 95% confidence level because their *P*-values are less than 0.05. The *P*-value for edge radius, which is close to 0.05, also suggests its significance. However, the axial relief angle and flute radius do not fit well with the model, indicating

Table 8 Analysis of variance (ANOVA) for the resultant cutting force

Source	DF	Adj SS	Adj MS	*F*-Value	*P*-Value
Model	**46**	**36,512,677**	**793,754**	**5.69**	**0.000**
Blocks	2	234,485	117,243	0.84	0.438
Linear	8	20,657,964	2,582,245	18.51	0.000
Core diameter (CD)	1	1,198,278	1,198,278	8.59	0.005
Radial rake angle (RRaA)	1	2,303,692	2,303,692	16.51	0.000
Helix angle (HA)	1	1,114,277	1,114,277	7.99	0.007
Radial relief angle (RReA)	1	9,983,245	9,983,245	71.56	0.000
Axial relief angle (ARA)	1	125,811	125,811	0.90	0.347
Edge radius (ER)	1	576,746	576,746	4.13	0.047
Flute radius (FR)	1	90,044	90,044	0.65	0.426
Width of the land (WL)	1	1,374,048	1,374,048	9.85	0.003
Square	8	2,625,816	328,227	2.35	0.031
Core diameter*Core diameter	1	21,001	21,001	0.15	0.700
Radial rake angle*Radial rake angle	1	58,306	58,306	0.42	0.521
Helix angle*Helix angle	1	5687	5687	0.04	0.841
Radial relief angle*Radial relief angle	1	11,941	11,941	0.09	0.771
Axial relief angle*Axial relief angle	1	4896	4896	0.04	0.852
Edge radius*Edge radius	1	13,497	13,497	0.10	0.757
Flute radius*Flute radius	1	247	247	0.00	0.967
Width of the land*Width of the land	1	5872	5872	0.04	0.838
2-Way interaction	28	11,657,575	416,342	2.98	0.000
Core diameter*Radial rake angle	1	105,868	105,868	0.76	0.388
Core diameter*Helix angle	1	34,914	34,914	0.25	0.619
Core diameter*Radial relief angle	1	832,908	832,908	5.97	0.018
Core diameter*Axial relief angle	1	143,752	143,752	1.03	0.315
Core diameter*Edge radius	1	112,972	112,972	0.81	0.373
Core diameter*Flute radius	1	4774	4774	0.03	0.854
Core diameter*Width of the land	1	243,908	243,908	1.75	0.192
Radial rake angle*Helix angle	1	394,712	394,712	2.83	0.099
Radial rake angle*Radial relief angle	1	1,524,368	1,524,368	10.93	0.002
Radial rake angle*Axial relief angle	1	19,520	19,520	0.14	0.710
Radial rake angle*Edge radius	1	430,847	430,847	3.09	0.085
Radial rake angle*Flute radius	1	11,257	11,257	0.08	0.778
Radial RAKE angle*Width of the land	1	42,363	42,363	0.30	0.584
Helix angle*Radial relief angle	1	442,624	442,624	3.17	0.081
Helix angle*Axial relief angle	1	6139	6139	0.04	0.835
Helix angle*Edge radius	1	202,618	202,618	1.45	0.234
Helix angle*Flute radius	1	2754	2754	0.02	0.889
Helix angle*Width of the land	1	24,602	24,602	0.18	0.676
Radial relief angle*Axial relief angle	1	21,730	21,730	0.16	0.695
Radial relief angle*Edge radius	1	293,672	293,672	2.10	0.153
Radial relief angle*Fluteradius	1	41,827	41,827	0.30	0.586
Radial relief angle*Width of the land	1	1,250,440	1,250,440	8.96	0.004
Axial relief angle*Edge radius	1	37,407	37,407	0.27	0.607
Axial relief angle*Flute radius	1	169,091	169,091	1.21	0.276
Axial relief angle*Width of the land	1	155,239	155,239	1.11	0.297
Edge radius*Flute radius	1	2066	2066	0.01	0.904
Edge radius*Width of the land	1	284,288	284,288	2.04	0.160
Flute radius*Width of the land	1	23,588	23,588	0.17	0.683
Error	50	6,975,902	139,518	–	–
Lack-of-fit	37	6,975,902	188,538		
Pure error	13	0	0		
Total	96	43,488,579			

Model summary = S: 373.521, R-sq: 83.96%, R-sq(adj) 69,92%

When the P-Value is lower than the predetermined significance level, it is typically highlighted in bold

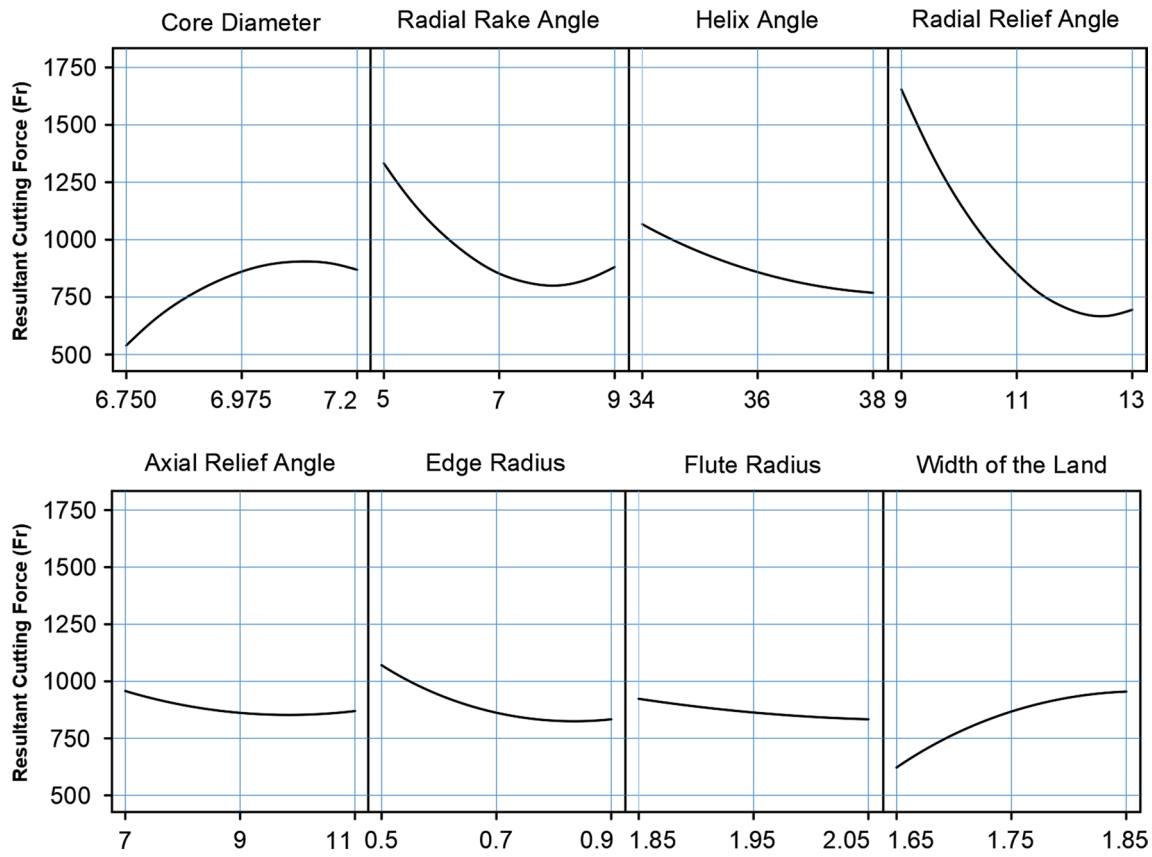

Fig. 4 Main effect plots for resultant cutting force (F_r)

no significant effect on the resultant cutting force. These parameters also negatively impact model adequacy and accuracy.

Figure 4 illustrates the main effect plot for the resultant cutting force and the design factors investigated. This figure also aids in identifying significant effects. The R^2 value, which measures the proportion of total variability explained by the model, is 0.8396 (83.96%). The adjusted R^2 value, useful for comparing models with different numbers of terms, is 0.6992 (69.92%). This result indicates that the adjusted R^2 value is close to the ordinary R^2 value and nearly 0.7, meeting the conditions for model adequacy. This analysis demonstrates that the developed model for the resultant cutting force can effectively navigate the design space within the experimental region.

The final empirical model that predicts resultant cutting force in terms of coded factors without performing any transformation on the response is represented in Eq. (8).

$$
\begin{aligned}
Fr = {} & -147586 + 45006CD - 1774 * RRaA - 1011 * HA - 104 * RReA + 583 * ARA - 11161 * ER \\
& - 6324 * FR + 27092 * WL - 3007 * CD * CD + 63.2 * RRaA + RRaA + 14.4 * HA * HA + 80 * Rrea * Rrea \\
& + 13.3 * ARA * ARA + 2213 * ER * ER + 1197 * FR * FR - 8043 * WL * WL - 114 * CD * RRaa - 57 * CD * HA \\
& - 305 * CD * Rrea - 145 * CD * ARA - 1229 * CD * ER + 423 * CD * FR + 2980 * CD * WL + 22.7 * RRaA \\
& * HA + 46.4 * RRaA * RreA - 5.6 * RRaA * ARA + 261 * RRaA * ER - 71 * RRaA * FR + 145 * RRaA * WL \\
& + 27.8 * HA * RreA + 2.7 * HA * ARA + 151 * HA * ER - 43 * HA * FR - 122 * HA * WL + 5.8 * RreA * ARA \\
& + 202.RreA * ER + 170 * RreA * FR - 925 * RreA * WL - 74 * ARA * ER + 281 * ARA * FR - 260 * ARA * WL \\
& + 314 * ER * FR + 3771 * ER * WL - 2451 * FR * WL
\end{aligned}
\tag{8}
$$

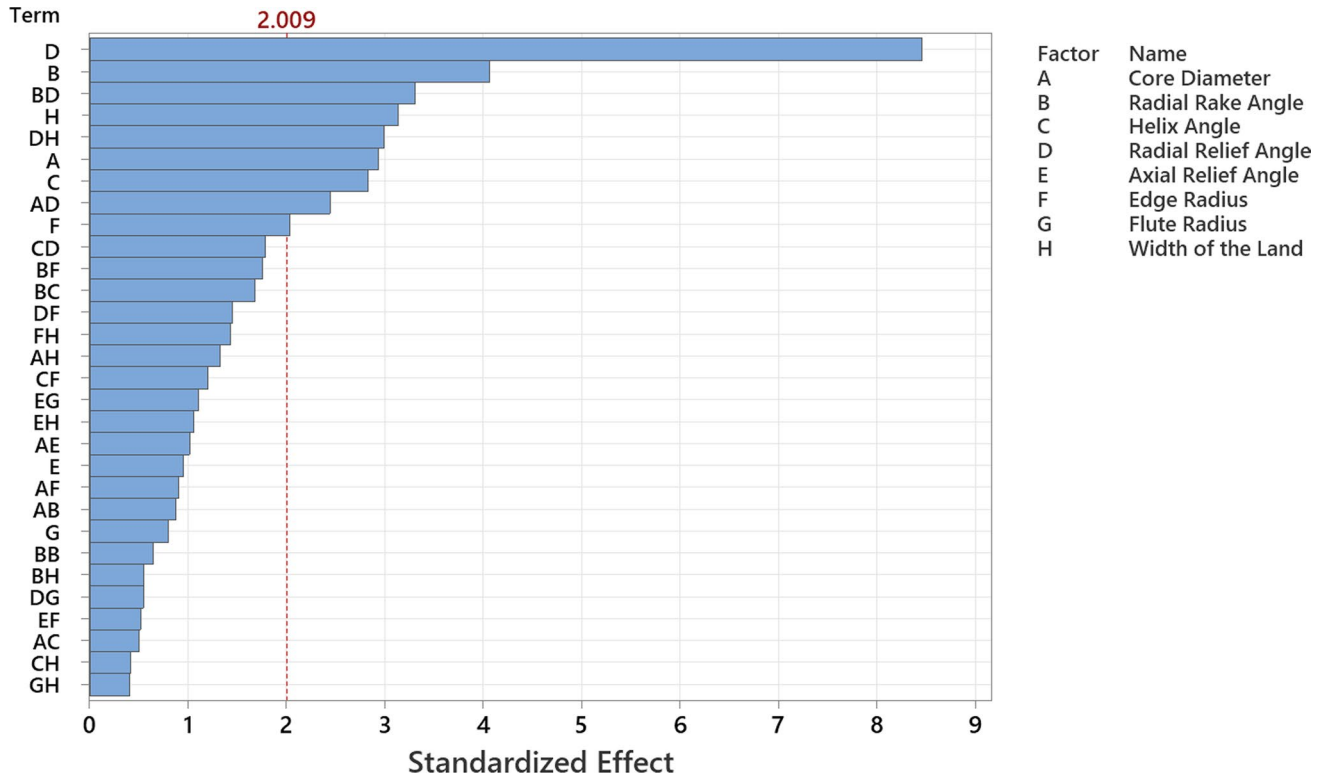

Fig. 5 Pareto chart of the standardized effects for F_r (only 30 effects shown)

Pareto charts are used to identify and prioritize the most important factors contributing to a problem [63]. On the other hand, experimental design utilizes main effects plots to comprehend the individual impact of factors on a response variable [64, 65]. Both a main effects plot and a Pareto plot are employed to identify key process parameters or factors that influence variability. The Pareto chart illustrates the standardized effect of independent variables and their interactions on overall desirability, whereas the main effects plot demonstrates the impact of independent variables [66]. The key difference lies in their applications and the types of analyses they support. In this regard, the main effect plots are presented in Fig. 4. These plots, created for the resultant cutting force, were analyzed under constant machining conditions and within the range of parameters where the cutting tool variables were determined. Two parameters significantly affected the resultant cutting force: the radial relief angle and the radial rake angle. It has been observed that the resultant cutting force only increases when the values of the width of the land and core diameter parameters increase. Conversely, increasing other cutting tool parameters within the determined range has a decreasing effect on the resultant cutting force.

The analysis shows that the radial relief angle and radial rake angle, which are the two most crucial tool parameters, have the most significant impact on the cutting forces. To enhance clarity in presenting the results from the analysis, Fig. 5 displays the Pareto chart of standardized effects. This chart emphatically reaffirms the pivotal role of the radial relief angle and radial rake angle parameters, asserting that they are the most critical design parameters. Subsequently, the width of the land and core diameter emerge as other design parameters with relative significance, in that order. Notably, the combination of the two parameters with the highest individual impact is also the most pronounced.

Figure 6 depicts the normal probability plot of the residuals. Examination of the plot indicates that the residuals predominantly align along a straight line, suggesting a normal distribution of errors. This observation confirms the proposed model's adequacy, indicating no apparent violations of the assumptions of independence or constant variance.

The resultant cutting force was assessed through finite element analysis. A contour plot, a two-dimensional visualization where points sharing the same response value are connected to form contour lines, is used to effectively delineate the relationship between two continuous variables and their corresponding responses [67]. Figure 7 illustrates combinations of tool parameters through contour plots, facilitating an analysis of their impact on the resultant cutting force. These plots clearly show the relationships between two cutting tool parameters and the resultant cutting force, making the optimal selection ranges for values of cutting tool

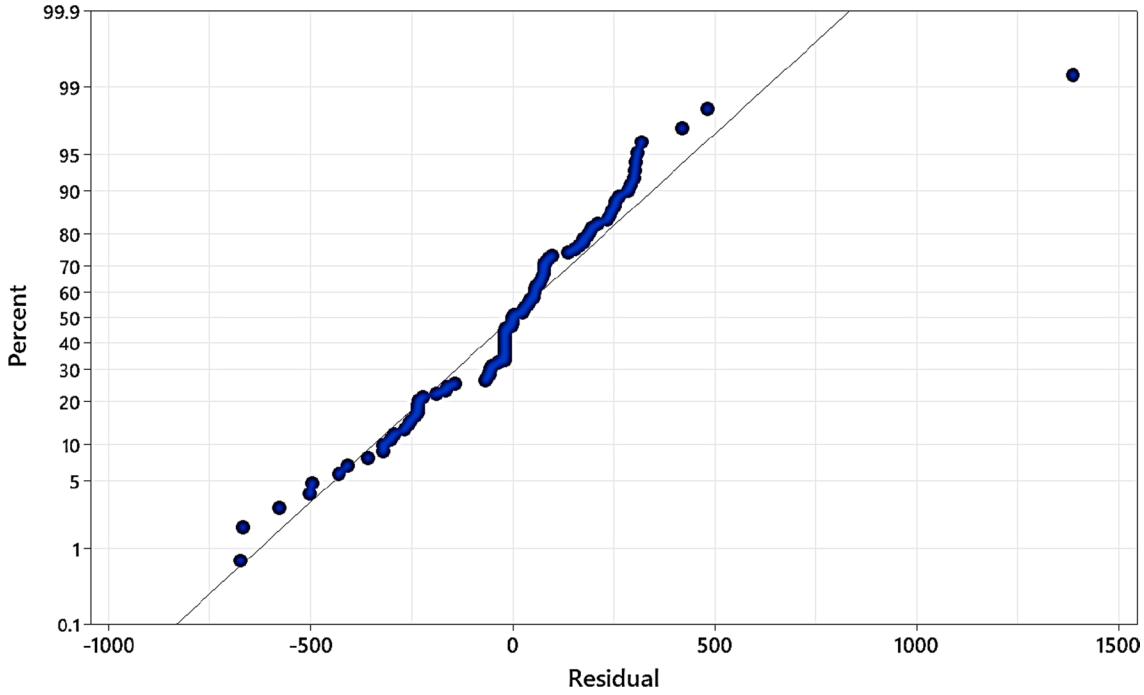

Fig. 6 Normal probability plot of F_r

parameters, which are conducive to optimizing the cutting force, comprehensible. The term "hold values" refers to the optimal tool parameters that yield the minimum resultant cutting force, achieved through response optimization for each binary interaction graph.

In the analysis of cutting tool parameters using graphical representations, the alignment parallel to the *X* or *Y* axes suggests that certain parameters significantly influence the resultant cutting force, with the radial relief angle having the most pronounced effect. Graphs show that as the influence of a parameter decreases, the correlation with cutting force weakens, often displaying no clear relationship. Differences in slopes or angles between axes indicate distinct impacts of the parameters, with some showing inverse proportional relationships where cutting force decreases as one parameter increases and another decreases. Conversely, combinations with minimal parameter impact, such as flute radius and core diameter, fail to produce clear, segmentable regions, indicating weak or non-existent relationships.

An optimal cutting tool can be manufactured by adopting values situated within the region corresponding to the lowest cutting force. Considering tolerances and manufacturability considerations in tool production, a range of optimal values specific to the region would prove more practical than a precise singular value. The hierarchical order—with radial relief angle being the most influential, followed by radial rake angle, width of the land, core diameter, helix angle, edge radius, axial relief angle, and flute radius—sheds light on the complex dynamics of machining performance.

In this comprehensive study on end mill tool geometry parameters and their impact on cutting forces, the radial relief angle and radial rake angle have been identified as the foremost contributors to achieving lower cutting forces. Figure 8 displays the contour plot and surface plot depicting these parameters, which stand out as the two most critical among the end mill tool's design parameters. These parameters, exerting the highest impact on the total resultant cutting force, exhibit a direct proportionality and functional relationship.

Analysis of the effect of the radial rake angle on the resultant cutting force showed that as the value of this parameter increased, the resultant cutting force first decreased from 5 degrees to around 7 degrees, then relatively increased toward 9 degrees. The increase in radial rake angle, which directly enhances the strength and sharpness of the edge of the end mill tool, can be associated with the decrease in the resultant cutting force [19, 68–70]. Increasing the value also reduces the plastic deformation of the rake surface of the end mill tool and the friction force of the chip flowing over the rake surface, thereby increasing tool life [5, 68, 69, 71]. A positive rake angle indicates a higher shear angle, which helps to reduce cutting forces and vibration [21]. However, too high a rake angle will also weaken the end mill tool. The weakening of the teeth may lead to an increase in the contact area between the end milling tool and the workpiece, explaining the subsequent relative increase. Furthermore, a larger value also leads to lower cutting tool strength and even creates the possibility of edge collapse [68, 69].

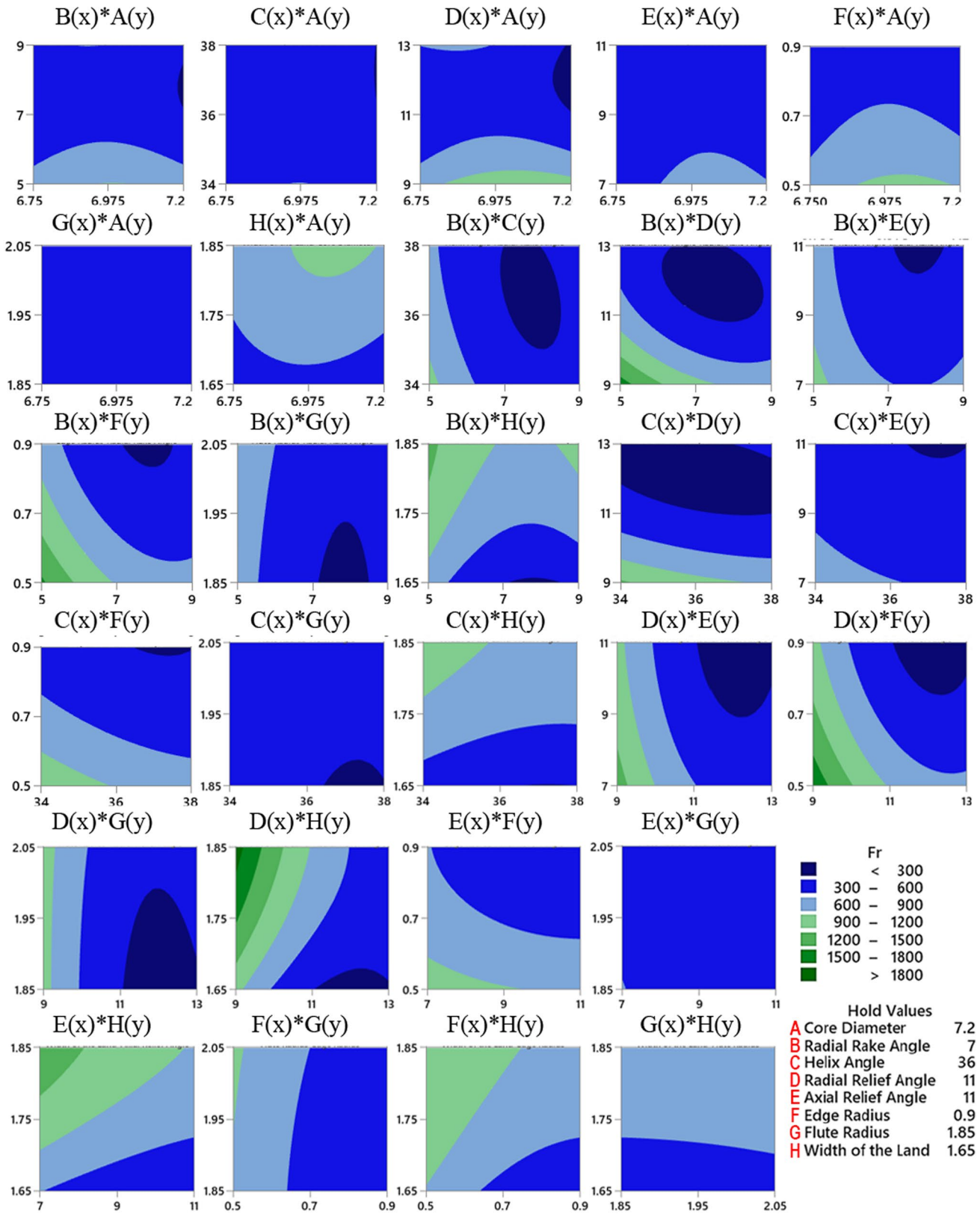

Fig. 7 Contour plots of F_r

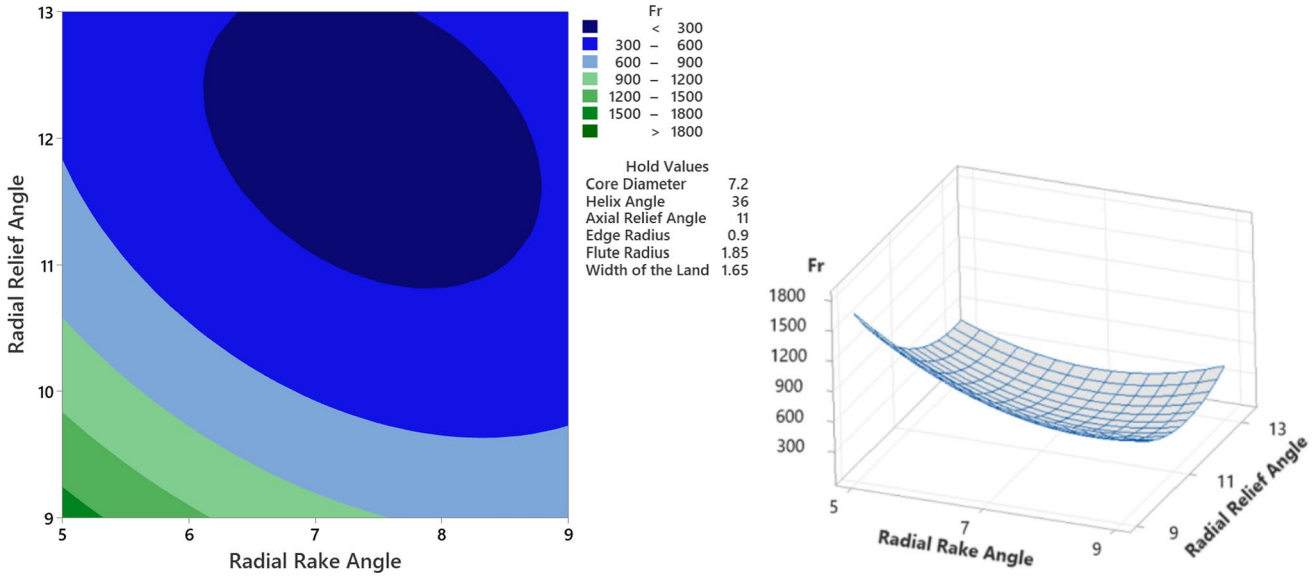

Fig. 8 Contour plot and surface plot of F_r, vs Radial relief angle, Radial rake angle

The radial relief angle causes friction between the mill end surface and the workpiece [26, 68]. Increasing the radial relief angle from 9 to 13 degrees resulted in a clear decrease in cutting forces. Reducing the radial relief angle generally results in increased chipping and cutting force because tool wear has a significant effect on the cutting force, and as the radial relief angle decreases, tool wear also increases [20]. Increasing the radial relief angle can sharpen the cutting edge and have a friction-reducing effect; however, in some cases, very high values may reduce the strength of the cutting edge and negatively affect heat dissipation from the tool [20, 26, 68]. Therefore, if the material does not optimize high radial relief angle values, it will shorten the tool's life. This reason accounts for the estimation of a relative upward trend in the radial relief angle value around and beyond 13 degrees.

Although other end mill tool geometry parameters are very important for the overall tool shape and stability, it was concluded that their impact on cutting forces when milling 316L stainless steel is relatively low. The characteristics of the material, such as its tendency to work-harden and generate long, stringy chips, are likely to have a significant impact on chip evacuation (which is affected by radial relief and radial rake angles) and shearing action (which is affected by radial rake angle), which are crucial aspects of determining cutting forces [72, 73].

Optimizing milling processes to reduce resultant cutting forces and designing end mill tools accordingly offer multifaceted advantages, including improved efficiency, longer tool life, enhanced surface finish, and cost savings. Response optimization will precisely determine the optimal parameters for the end milling tool that produce the minimum resultant cutting force, in line with the analyses. This process involves a desirability function that reaches a maximum value within the range of 0–1, as defined by Derringer and Suich [74]. This method is appealing for the industry as it addresses various quality characteristic challenges [75]. The method employs an objective function, D(X), known as the desirability function, which converts an estimated response into a scale-independent value termed the desirability value (d_i). The desirability function is optimized using a gradient-based method, and if its value is 1 or close to 1, the response is accepted. Conversely, if it is close to 0, the response is completely rejected [76, 77]. Numerical optimization determines a point that maximizes the desirability function using a mathematical method [78]. The composite desirability is calculated as the weighted geometric mean of the individual desirabilities for the responses.

To maximize a response, the desirability is calculated as follows [79]:

$$\begin{aligned} d_i &= 0 && \hat{y}_i < L_i \\ d_i &= \left(\left(\hat{y}_i - L_i\right)/\left(T_i - L_i\right)\right)^{r_i} && L_i \le \hat{y}_i \le T_i \\ d_i &= 1 && \hat{y}_i > T_i \end{aligned} \tag{9}$$

To minimize a response, the desirability is calculated as follows:

$$\begin{aligned} d_i &= 0 && \hat{y}_i > U_i \\ d_i &= \left(\left(U_i - \hat{y}_i\right)/\left(U_i - T_i\right)\right)^{r_i} && T_i \le \hat{y}_i \le U_i \\ d_i &= 1 && \hat{y}_i > T_i \end{aligned} \tag{10}$$

To target a response, the desirability is calculated as follows:

$$\begin{aligned} d_i &= \left(\left(\hat{y}_i - L_i\right)/\left(T_i - L_i\right)\right)^{r_i} \quad L_i \le \hat{y}_i \le T_i \\ d_i &= \left(\left(U_i - \hat{y}_i\right)/\left(U_i - T_i\right)\right)^{r_i} \quad T_i \le \hat{y}_i \le U_i \\ d_i &= 0 \qquad\qquad\qquad\qquad\quad \hat{y}_i < L_i \\ d_i &= 0 \qquad\qquad\qquad\qquad\quad \hat{y}_i > U_i \end{aligned} \tag{11}$$

The composite desirability is calculated using the weighted geometric mean of individual desirabilities. The formula for composite desirability is as follows [79]:

$$D = \left(\prod \left(d_i^{w_i}\right)\right)^{\frac{1}{W}} \tag{12}$$

If the importance assigned to each response is equal, the composite desirability is calculated as follows [79]:

$$D = \left(d_1 x d_2 x \ldots x d_n\right)^{\frac{1}{n}} \tag{13}$$

where , $\hat{y}_i$ predicted value of ith response, T_i target value of ith response, L_i lowest acceptable value for ith response, U_i highest acceptable value for ith response, d_i individual desirability for ith response, D composite desirability, r_i weight of desirability function of ith response, w_i importance of ith response, $Wis \sum w_i$, n number of responses.

In this study, among the three types of individual desirability functions, "the smaller is better" was preferred because the goal is to achieve a low resultant cutting force. Both Table 9 and Fig. 9 present the optimum end mill tool design parameters. The transformation of response scales to a zero-to-one desirability scale was influenced by the relative weight assigned to each response. This weight, selected from a range of 0.1–10, determined how desirability was distributed between the lower (or upper) bound and the target value. A weight of 1 indicated equal importance placed on both the target and the bounds, representing a neutral setting. Adjusting the weight above 1 placed more emphasis on achieving the target, requiring responses to move closer to it for a specified desirability. The weight parameters were not changed, and the default neutral value was used. The best endmill tool parameter values that come from response optimization are about 70% accurate when compared to the closest tool parameters using the full factorial predictive approach. The desirability value was identified as 1, and the composite desirability was likewise determined to be 1. All desirability values were verified to be 1, affirming that the response could be unequivocally accepted.

Table 9 Response optimization and the best end mill tool geometry parameters based on the F_r

Test no	Core diameter	Radial rake angle	Helix angle	Radial relief angle	Axial relief angle	Edge radius	Flute radius	Width of the land	Predicted F_r
$A_3B_2C_3D_3E_3F_3G_1H_3$	7.2	7	34	13	11	0.9	1.85	1.65	288.73

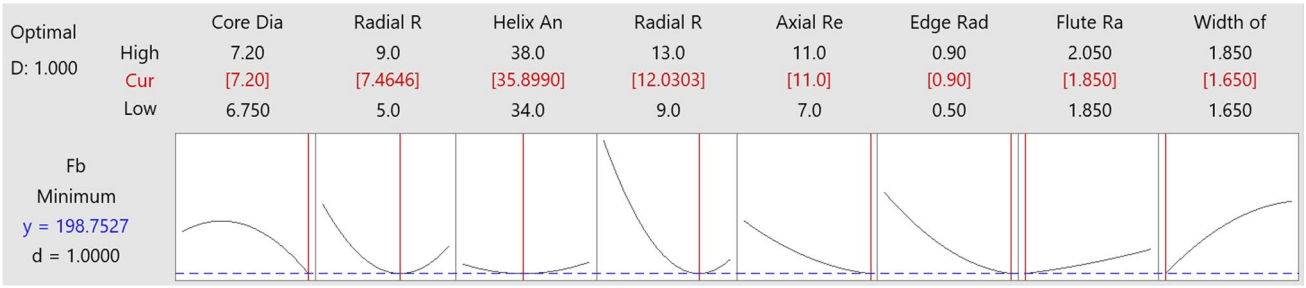

Fig. 9 Response optimization plot for F_r

4 Conclusions

In this current investigation, the primary focus centers on optimizing end milling tool geometry parameters specifically tailored for machining 316L material, aiming to achieve the lowest total resultant cutting force. Employing the FEA-RSM-ANOVA-Response Optimization approach, the study systematically determined the most effective tool geometry parameters. Comprehensive design data, derived from thorough analyses and numerical outcomes, provided valuable insights into the intricate dynamics of the end milling process for 316L material. The study yields the following conclusions:

1. The statistical analysis, including ANOVA and the *F*-ratio test, supports the adequacy and significance of the proposed quadratic model for the resultant cutting force, as evidenced by a *P*-value below 0.05 and an *F*-ratio exceeding the standard value.
2. Radial relief angle and radial rake angle are identified as the most significant parameters based on their *P*-values, while the axial relief angle and flute radius, not aligning with the model, impact its adequacy. Therefore, it has been demonstrated that the radial relief angle and radial rake angle play a critical role in reducing cutting forces when end milling 316L stainless steel.
3. Despite the axial relief angle and flute radius having a non-significant effect on the resultant cutting force, the overall model, with an R^2 value of 83.96% and an adjusted R^2 value of 69.92%, demonstrates high explanatory power within the experimental region, affirming its suitability for navigating the design space.
4. The process of optimizing the end milling tool's design parameters through response optimization using the desirability function provided accurate values to minimize the cutting force. The composite desirability value also confirmed that the response was considered definitive, underscoring the success of the optimization process. It is recognized that optimum tool parameters, obtained with relatively high accuracy, will enhance productivity, surface quality, and cost savings.
5. The unique properties of the material highlight the importance of customized tool designs and the need for material-specific optimization in the design of end milling tools to achieve the best possible machining performance.

These findings provide valuable information for redesigning cutting tool geometries for specific applications and ultimately contribute to improving machining efficiency and precision. Further research can delve deeper into the complex relationships between these parameters, enabling continuous improvement and optimization of end mill tool geometry parameters for improved machining results.

Acknowledgments The findings and insights presented in this study have been derived from the PhD thesis of Marmara University. Additionally, the authors would like to thank all the stakeholders of this project and particularly the engineers and technicians of the Karcan Cutting Tools Industry & Trade Inc. Co. Where our research was conducted

Data availability Data associated with this study are recorded.

Declarations

Conflict of interest The authors declare no competing interests.

Consent to participate The authors claim that none of the contents in this manuscript has been published or considered for publication elsewhere.

Consent for publication The editor has my (authors) consent to publish.

References

1. Masmiati N, Sarhan AA (2015) Optimizing cutting parameters in inclined end milling for minimum surface residual stress–Taguchi approach. Measurement 60:267–275

2. Zhou L, Li J, Li F, Mendis G, Sutherland JW (2018) Optimization parameters for energy efficiency in end milling. Proc CIRP 69:312–317
3. Wu B, Yan X, Luo M, Gao G (2013) Cutting force prediction for circular end milling process. Chin J Aeronaut 26(4):1057–1063
4. Ciurana J (2014) Designing, prototyping and manufacturing medical devices: an overview. Comput Integr Manuf 27(10):901–918
5. Daniyan I, Tlhabadira I, Daramola O, Mpofu K (2019) Design and optimization of machining parameters for effective AISI P20 removal rate during milling operation. Proc CIRP 84:861–867
6. Vobrouček J (2015) The influence of milling tool geometry on the quality of the machined surface. Proc Eng 100:1556–1561
7. Singh K (1992) Optimization of machining parameters in milling. University of British Columbia, Columbia
8. Prasad K, Chakraborty S (2016) A knowledge-based system for end mill selection. Adv Prod Eng Manag 11(1):15
9. Akamatsu T, Kitajima K, Minamino S, Kiriyama T (2005) Influence of material of small radius ball end mill on cutting accuracy in deep precision machining. Key Eng Mater 291:471–474
10. Plodzien M, Burek J, Zylka L, Sulkowicz P (2020) The influence of end mill helix angle on high performance milling process. J Mech Sci Technol 34:817–827
11. Kim JH, Park JW, Ko TJ (2008) End mill design and machining via cutting simulation. Comput Aided Des 40(3):324–333
12. Korkut I, Donertas M (2007) The influence of feed rate and cutting speed on the cutting forces, surface roughness and tool–chip contact length during face milling. Mater Des 28(1):308–312
13. Sultan AA, Okafor AC (2016) Effects of geometric parameters of wavy-edge bull-nose helical end-mill on cutting force prediction in end-milling of Inconel 718 under MQL cooling strategy. J Manuf Process 23:102–114
14. Duan Z, Li C, Ding W, Zhang Y, Yang M, Gao T, Cao H, Xu X, Wang D, Mao C (2021) Milling force model for aviation aluminum alloy: academic insight and perspective analysis. Chin J Mech Eng 34(1):1–35
15. Magnevall M, Lundblad M, Ahlin K, Broman G (2012) High frequency measurements of cutting forces in milling by inverse filtering. Mach Sci Technol 16(4):487–500
16 Zhu K (2021) Smart machining systems: modelling, monitoring and informatics. Springer International Publishing, Cham
17. Joshi SN, Bolar G (2021) Influence of end mill geometry on milling force and surface integrity while machining low rigidity parts. J Inst Eng (India) 102(6):1503–1511
18. Ren J, Zhou J, Wei J (2015) Optimization of cutter geometric parameters in end milling of titanium alloy using the grey-Taguchi method. Adv Mech Eng 7(2):721093
19. Sethupathy A, Shanmugasundaram N (2021) Prediction of cutting force based on machining parameters on AL7075-T6 aluminum alloy by response surface methodology in end milling. Materwiss Werksttech 52(8):879–890
20. Ma J-w, Jia Z-y, He G-z, Liu Z, Zhao X-x, Qin F-z (2019) Influence of cutting tool geometrical parameters on tool wear in high-speed milling of Inconel 718 curved surface. Proc Inst Mech Eng B J Eng Manuf 233(1):18–30
21. Subramanian M, Sakthivel M, Sooryaprakash K, Sudhakaran R (2013) Optimization of end mill tool geometry parameters for Al7075-T6 machining operations based on vibration amplitude by response surface methodology. Measurement 46(10):4005–4022
22. Aslantas K, Alatrushi L (2021) Experimental study on the effect of cutting tool geometry in micro-milling of Inconel 718. Arab J Sci Eng 46(3):2327–2342
23. Tang J, Deng C, Chen X, Zhai H (2023) Analysis and optimization of milling deformations of TC4 alloy Thin-walled parts based on finite element simulations. Machines 11(6):628
24. Ji J, Yang Q, Chen P, Lu K, Wu Y (2021) An improved mathematical model of cutting temperature in end milling Al7050 based on the influence of tool geometry parameters and milling parameters. Math Probl Eng 2021:1–10
25. Ahmed F, Kumaran ST, Ahmad F (2022) Analysis of wear mechanisms and chip morphology during machining of tool steel using TiAlSiCrN-Coated WC-Co ball end mills. Res Sq https://doi.org/10.21203/rs.3.rs-1144076/v1
26. Zhang X, Zhang J, Zhou H, Ren Y, Xu M (2018) A novel milling force model based on the influence of tool geometric parameters in end milling. Adv Mech Eng 10(9):1687814018798185
27. Wang L, Lin B, Guo Y, Yao JM (2016) Optimization of end mill geometry parameters based on oblique cutting theory. Key Eng Mater 693:850–855
28. Doluk E, Rudawska A (2022) Effect of Machining settings and tool geometry on surface quality after machining of Al/CFRP sandwich structures. Adv Sci Technol Res J 16(3):22–33
29. DaneshNarooei K, Ramli R (2022) Optimal selection of cutting parameters for surface roughness in milling machining of AA6061-T6. Int J Eng 35(6):1170–1177
30. Izamshah R, Rafiq M, Lamat A, Kasim M, Salleh M, Liew P, Aziz M, Abdullah R (2021) Effects of cutter geometry and cutting parameters on machining Al/SiC metal matrix composites (MMC). Int J Nanoelectron Mater 14:343–352
31. Monka PP, Monkova K, Majstorovic VD, Božić Ž, Andrej A (2021) Optimal cutting parameter specification of newly designed milling tools based on the frequency monitoring. Int J Adv Manuf Technol 115:777–794
32 Zhang H-J, Sun C, Liua M, Gao F (2018) Analysis of the optimization of tool geometric parameters for milling of Inconel718. IOP Conf Series Mater Sci Eng 423:012030
33. Kusyi Y, Kuk A, Topilnytskyy V, Rebot D, Bojko M (2021) Influence of constructive and geometric parameters of the end cutters on the microprofile characteristics of casting surfaces. Technol Audit Prod Reserves 2(1):58
34. Asghari S (2019) Innovative cutting tool design for machining advanced engineering materials. University of Bath, UK
35. Arrazola PJ, Özel T, Umbrello D, Davies M, Jawahir IS (2013) Recent advances in modelling of metal machining processes. CIRP Ann 62(2):695–718
36. Li JN, Gao D, Lu Y, Hao ZP, Wang ZQ (2022) Mechanical properties and microstructure evolution of additive manufactured 316L stainless steel under dynamic loading. Mater Sci Eng A 855:143896
37. Duriagina Z (2019) Stainless Steels and Alloys. IntechOpen.
38. Ozturk M, Roy A, Bhat RA, Sukan FV, Tonelli FMP (2023) Synthesis of bionanomaterials for biomedical applications. Elsevier Science, Amsterdam
39. Dhanachezian M, Tinesh T, Paul S, Roy I (2016) Study of machinability characteristics for turning austenitic (316L) and super duplex (2505) stainless stell using PVD-TiAlN nano-multilayer inserts. J Eng Appl Sci 11(2):1262–1268
40. Xi T, Shahzad MB, Xu D, Sun Z, Zhao J, Yang C, Qi M, Yang K (2017) Effect of copper addition on mechanical properties, corrosion resistance and antibacterial property of 316L stainless steel. Mater Sci Eng C 71:1079–1085
41. Yasir M, Ginta TL, Ariwahjoedi B, Alkali AU, Danish M (2016) Effect of cutting speed and feed rate on surface roughness of AISI 316l SS using end-milling. ARPN J Eng Appl Sci 11(4):2496–2500
42. Nasr MNA, Ng EG, Elbestawi MA (2007) Modelling the effects of tool-edge radius on residual stresses when orthogonal cutting AISI 316L. Int J Mach Tools Manuf 47(2):401–411
43. Equbal A, Equbal MA, Equbal MI, Ravindrannair P, Khan ZA, Badruddin IA, Kamangar S, Tirth V, Javed S, Kittur M (2022)

Evaluating CNC milling performance for machining AISI 316 stainless steel with carbide cutting tool insert. Mater 15(22):8051
44. AdvantEdge (2024) AdvantEdge Cutting Edge FEA. https://thirdwavesys.com/machining-modeling/advantedge.
45. Naik R, Kumar UA, P L, (2020) Experimental Investigation on surface roughness, hardness and mrr of stainless steel 316L in EDM with distilled water as electrolyte using taguchi method. Int J Sci Eng Res 7:274–280
46. Esmaeilbeigi M, BehzadiTayemeh M, Johari SA, Ghorbani F, Sourinejad I, Yu IJ (2022) In silico modeling of the antagonistic effect of mercuric chloride and silver nanoparticles on the mortality rate of zebrafish (*Danio rerio*) based on response surface methodology. Environ Sci Pollut Res 29(36):54733–54744
47. Bezerra MA, Santelli RE, Oliveira EP, Villar LS, Escaleira LA (2008) Response surface methodology (RSM) as a tool for optimization in analytical chemistry. Talanta 76(5):965–977
48. Rahimi-Gorji M, Pourmehran O, Hatami M, Ganji D (2015) Statistical optimization of microchannel heat sink (MCHS) geometry cooled by different nanofluids using RSM analysis. Eur Phys J Plus 130:1–21
49. Myers RH, Montgomery DC, Anderson-Cook CM (2016) Response surface methodology: process and product optimization using designed experiments. Wiley, Hoboken
50. Shirazi M, Khademalrasoul A, SafieddinArdebili SM (2020) Multi-objective optimization of soil erosion parameters using response surface method (RSM) in the Emamzadeh watershed. Acta Geophys 68:505–517
51. Lafifi B, Rouaiguia A, Boumazza N (2019) Optimization of geotechnical parameters using Taguchi's design of experiment (DOE), RSM and desirability function. Innov Infrastruct Solut 4(1):35
52. Khuri AI, Mukhopadhyay S (2010) Response surface methodology. Wiley Interdiscip Rev Comput Stat 2(2):128–149
53. Routara B, Bandyopadhyay A, Sahoo P (2009) Roughness modeling and optimization in CNC end milling using response surface method: effect of workpiece material variation. Int J Adv Manuf Technol 40:1166–1180
54. Gaitonde V, Karnik S, Rubio JC, Correia AE, Abrão A, Davim JP (2008) Analysis of parametric influence on delamination in high-speed drilling of carbon fiber reinforced plastic composites. J Mater Process Technol 203:431–438
55. Nanda A, Mohapatra BB, Mahapatra APK, Mahapatra APK, Mahapatra APK (2021) Multiple comparison test by Tukey's honestly significant difference (HSD): do the confident level control type I error. Int J Appl Math Stat 6(1):59–65
56. Singh H, Halder N, Singh B, Singh J, Sharma S, Shacham-Diamand Y (2023) Smart farming revolution: portable and real-time soil nitrogen and phosphorus monitoring for sustainable agriculture. Sensors 23(13):5914
57. Abd Rahman H, Khalid ZM, Ismail NM, Kamisan NAB, Norrulashikin SM, Nor SRM, Shabri A, Hamdan MF (2022) Statistical analysis on students' evaluation and students' final exam marks in undergraduate mathematical courses at universiti teknologi malaysia. Int J Adv Res Fut R Learn Educ 27(1):1–8
58. Dahiru T (2008) *P*-value, a true test of statistical significance? a cautionary note. Ann Ib Postgrad Med 6(1):21–26
59. Cumming G (2009) Inference by eye: reading the overlap of independent confidence intervals. Stat Med 28(2):205–220
60. Greenland S, Senn SJ, Rothman KJ, Carlin JB, Poole C, Goodman SN, Altman DG (2016) Statistical tests, *P* values, confidence intervals, and power: a guide to misinterpretations. Eur J Epidemiol 31:337–350
61. Ware JH, Mosteller F, Delgado F, Donnelly C, Ingelfinger JA (2019) P values, in Medical uses of statistics. CRC Press, Boca Raton, pp 181–200
62. Babu GP, Murthy B, Venkatarao K, Ratnam C (2017) Multi-response optimization in orthogonal turn milling by analyzing tool vibration and surface roughness using response surface methodology. Proc Inst Mech Eng B J Eng Manuf 231(12):2084–2093
63. Shari HA, Khalid N, Ashaari NS, Judi HM (2009) Statistical process control in plastic packaging manufacturing: a case study. Intern Conf Electrical Eng Inform IEEE 1:199–203
64. Ekpenyong MG, Antai SP, Asitok AD, Ekpo BO (2017) Plackett-Burman design and response surface optimization of medium trace nutrients for glycolipopeptide biosurfactant production. Iran Biomed J 21(4):249
65. Moussa BA, Mahrouse MA, Fawzy MG (2021) Application of experimental design in HPLC method optimization and robustness for the simultaneous determination of canagliflozin, empagliflozin, linagliptin, and metformin in tablet. Biomed Chromatogr 35(10):e5155
66. LučićPotkonjak MN, SredovićIgnjatović I, Lević S, Dajić-Stevanović Z, Kolašinac S, Belović M, Torbica A, Zlatanović I, Pavlović V (2023) Influence of ultrasonic and chemical pretreatments on quality attributes of dried pepper (*Capsicum annuum*). Foods 12(13):2468
67. Minitab (2023) Overview for Contour Plot. https://support.minitab.com/en-us/minitab/21/helP-and-how-to/statistical-modeling/using-fitted-models/how-to/contour-plot/before-you-start/overview/.
68. Shuangyu W, Yuewei B, Xiang C 2010 CAD tool development of end mill parameter design based on DA method, In: International conference on mechanic automation and control engineering IEEE
69. Ren J, Zhou J, Zeng J (2016) Analysis and optimization of cutter geometric parameters for surface integrity in milling titanium alloy using a modified grey–Taguchi method. Proc Inst Mech Eng B J Eng Manuf 230(11):2114–2128
70. Suresh Kumar Reddy N, Venkateswara Rao P (2005) Selection of optimum tool geometry and cutting conditions using a surface roughness prediction model for end milling. Int J Adv Manuf Technol 26:1202–1210
71. Tamura S, Matsumura T (2021) Cutting force in milling of additive manufacturing AISI 420 stainless steel. ESAFORM. https://doi.org/10.25518/esaform21.1505
72. Sultan AZ, Sharif S, Kurniawan D (2020) Drilling of AISI 316L stainless steel: Effect of coolant condition on surface roughness and tool wear. In: AIP conference proceedings. AIP publishing.
73. Mukhtar M, Effendee M, Ibrahim MH, Syahrir M (2021) Analysis of solid carbide drilling performance on AISI 316L austenite stainless steel using MQL (minimum quantity lubrication) using peck drilling approach. J Phy Conf Series 1874(1):012065
74. Kshirsagar MP, Kalamkar VR, Pande RR (2020) Multi-response robust design optimization of natural draft biomass cook stove using response surface methodology and desirability function. Biomass Bioenerg 135:105507
75. Suresh P, Marimuthu K, Ranganathan S (2013) Modelling and analysis of process parameters on turning of aluminum hybrid composites P. Aust J Basic Appl Sci 7(9):341–353
76. Ozturk BA, Koksal G (2010) Weber GW. Optimization of desirability functions as a DNLP model by GAMS/BARON 1239:305–310
77. Ninggar Y, Anggoro P, Bawono B, Setyohad D, Tauviqirrahman M, Jamari J (2023) Optimization of parameter for cutting

condition of uhmwpe acetabular cup based on taguchi and desirability functions. Cogent Eng 10(1):2233247
78. Mesa L, Martínez Y, Barrio E, González E (2017) Desirability function for optimization of Dilute Acid pretreatment of sugarcane straw for ethanol production and preliminary economic analysis based in three fermentation configurations. Appl Energy 198:299–311
79. Bin Reyaz MS, Sinha AN (2023) Analysis of mechanical properties and optimization of tungsten inert gas welding parameters on dissimilar AA6061-T6 and AA7075-T6 by a response surface methodology-based desirability function approach. Eng Optim 1:36